Density-functional theory calculation of the intermolecular exchange interaction in the magnetic Mn$_4$ dimer

Kyungwha Park,[1,2,*] Mark R. Pederson,[1] Steven L. Richardson,[1,2] Nuria Aliaga-Alcalde,[3] and George Christou[3]

[1]*Center for Computational Materials Science, Code 6390, Naval Research Laboratory, Washington, DC 20375, USA*
[2]*Department of Electrical Engineering and Materials Science Research Center, Howard University, Washington, DC 20059, USA*
[3]*Department of Chemistry, University of Florida, Gainesville, Florida 32611, USA*

The dimeric form of the single-molecule magnet $[Mn_4O_3Cl_4(O_2CEt)_3(py)_3]_2$ recently revealed interesting phenomena: no quantum tunneling at zero field and tunneling before magnetic-field reversal. This is attributed to substantial antiferromagnetic exchange interaction between different monomers. The intermolecular exchange interaction, electronic structure, and magnetic properties of this molecular magnet are calculated using density-functional theory within generalized-gradient approximation. Calculations are in good agreement with experiment.

Single-molecule magnets (SMMs), such as $[Mn_{12}O_{12}(CH_3COO)_{16}(H_2O)_4]\cdot 2(CH_3COOH)\cdot 4(H_2O)$ (hereafter Mn_{12}) (Ref. 1) and $[Fe_8O_2(OH)_{12}(tacn)_6]Br_8 \cdot 9(H_2O)$ (hereafter Fe_8) (Ref. 2) have received tremendous attention due to macroscopic quantum tunneling[3] and possible use as nanomagnetic storage devices. Hysteresis loop measurements on the SMMs Mn_{12} and Fe_8 showed magnetization steps at low temperatures upon magnetic-field reversal.[4] This is due to quantum tunneling between spin-up states and spin-down states despite a large effective spin $S=10$ for each molecule. The resonant tunneling fields in these systems are primarily determined by the magnetomolecular anisotropy. Recently, a dimerized single-molecule magnet $[Mn_4O_3Cl_4(O_2CEt)_3(py)_3]_2$ (hereafter Mn_4 dimer), where $Et=CH_3CH_2^-$ and $py=C_5H_5N$, has been formed[5,6] which exhibited qualitatively different tunneling behavior: quantum tunneling prior to magnetic-field reversal and an absence of quantum tunneling at zero field in contrast to other SMMs such as Mn_{12} and Fe_8.[6] To understand the basis for the qualitative deviation, we have calculated both the magnetomolecular anisotropy and the intermolecular exchange interaction in the Mn_4 dimer using density-functional theory. Our results confirm that there exists an appreciable *antiferromagnetic* exchange interaction between monomers, and that tunneling fields in this dimer are strongly influenced by the presence of the monomer-monomer exchange interaction. This interaction produces a bias field that encourages monomeric magnetic-moment reversal below zero field and prevents two monomers from simultaneously flipping their magnetic moments at zero field. We determine that the origin of the exchange interaction is not dominated by either kinetic or exchange-correlation terms and that the total "exchange" interaction is, in fact, an order of magnitude smaller than the kinetic contribution. For Mn_{12} and Fe_8, the intermolecular exchange interaction has not been observed experimentally, and it is generally accepted that the overlap between neighboring molecules is negligible.

In this work, we discuss calculations on the Mn_4 dimer which is formed by inversion of the threefold symmetric monomer shown in Fig. 1. The magnetic core of the Mn_4 monomer consists of three ferromagnetically coupled Mn^{3+}

($S=2$) ions coupled antiferromagnetically to the remaining Mn^{4+} ($S=3/2$) ion leading to a total ground-state spin of $S=2\times3-3/2\times1=9/2$ (refer to Fig. 1). The core has a similar cubane structure as the inner core of the SMM Mn_{12}, although there are four Mn^{4+} for Mn_{12}. We investigate the electronic structure and magnetic properties of this SMM Mn_4 using density-functional theory (DFT). We calculate optimized geometries for the Mn_4 monomer and dimer, their
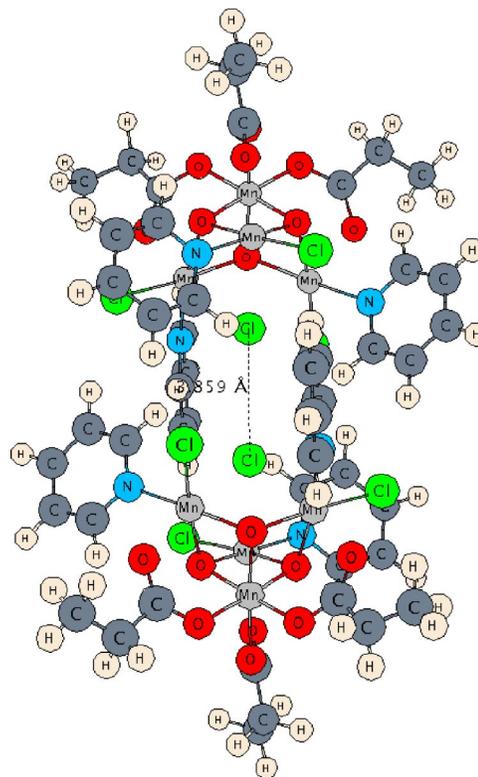

FIG. 1. (Color online) Mn_4 dimer geometry. The dimer is formed by inversion of the threefold symmetric monomer. Each monomer has a magnetic core consisting of three ferromagnetically coupled Mn^{3+} spins ($S=2$) coupled antiferromagnetically to one Mn^{4+} spin ($S=3/2$) ion leading to a total spin of $S=9/2$. The distance between the two central Cl atoms marked as the dotted line was measured to be 3.86 Å.

binding energy, the monomeric magnetic anisotropy barrier (MAE), and the exchange-coupling constant between monomers. Results are compared with experiment.

Our DFT calculations[7] are performed with the all-electron Gaussian-orbital-based Naval Research Laboratory Molecular Orbital Library (NRLMOL).[8] Here we use the Perdew-Burke-Ernzerhof (PBE) generalized-gradient approximation (GGA).[9] Before discussing energetics and magnetic phenomena, we discuss two structural issues. First, we have considered monomers and dimers that are terminated by both H and by the CH_2CH_3 radicals found in the experimental structure. Second, we have considered structures based on two conformers of the monomeric unit. While a complete vibrational analysis will be discussed in a later paper,[10] all indications are that both conformers are stable. The conformers have slightly different arrangements of the pyridine ligands. The first conformer was identified by a density-functional-based geometry optimization of the hydrogenated monomer. The second conformer was identified by improvements on the monomer deduced from the experimental x-ray data. In the remainder of the paper we refer to these monomers as the computationally determined conformer (CDC) and the experimentally determined conformer (EDC).

Each Mn_4 monomer has threefold symmetry, so there are 26 inequivalent atoms to consider. The number of inequivalent atoms is reduced to 20 when the CH_2CH_3 radical is replaced by H. A pyridine ring is initially constructed to lie in the plane defined by the vector connecting Mn^{3+} and neighboring N and the sum of the two vectors connecting Mn^{3+} with the two closest Cl's (refer to Fig. 1). The geometries for the pyridine ring and the cubane were first optimized separately to generate an initial geometry for the DFT calculations on the full monomer. The initial geometry for the monomer was relaxed using NRLMOL with the Cl atom fixed to reproduce the experimental Cl-Cl distance (3.86 Å) upon dimerization (i.e., adding inversion symmetry). Relaxation continues until the forces exerted on all atoms become ~0.001 Hartree/bohr. The CDC dimer is then obtained by inversion of the CDC monomer with the fixed value of d = 3.86 Å (marked as dotted in Fig. 1). For the case of the x-ray deduced experimental geometry, the C-H bond lengths are underestimated (0.71 Å–0.96 Å) in comparison to standard hydrogen bond lengths, which yields self-consistent forces on hydrogen atoms as large as 0.8 Hartree/bohr. To improve the experimental geometry, all hydrogen positions were first moved to create C-H bond lengths of 1.1 Å, and then additional optimization of the experimental geometry was performed with the Cl-Cl distance fixed. The experimental geometry without corrected hydrogen positions was 53 eV higher in energy than that of the structure with corrected hydrogen positions. Hereafter, unless we specify, the EDC monomer refers to the optimized experimental geometry with corrected hydrogen positions.

We have used full basis sets for all six different atoms and fine mesh.[11] Charges and magnetic moments for Mn's from the CDC monomer agree well with those from the EDC monomer. For example, a sphere with a radius of 2.23 bohr captures charges of 23.4 and 23.7, and magnetic moments of
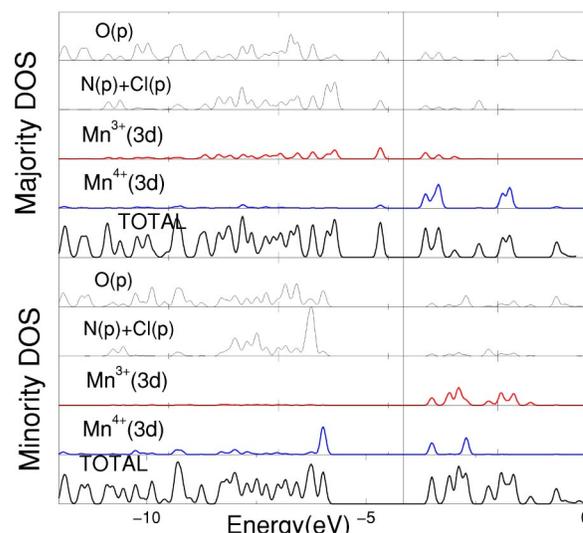

FIG. 2. (Color online) Electronic DOS for majority and minority spins for the Mn_4 monomer. Shown are projected $Mn(3d)$ DOS of the two types of Mn ions, projected p DOS of the three N atoms and the four Cl atoms, projected p DOS of the nine O atoms, and the total DOS defined by the sum of projected DOS of all atoms in the monomer. All projected DOS have the same scale which is different from that for the total DOS. The vertical line denotes the Fermi level. Directly below the Fermi level, for majority spins the projected $Mn^{3+}(3d)$ DOS has more weight than the $Mn^{4+}(3d)$ DOS. For minority spins, the tendency is the opposite.

$3.6\mu_B$ and $-2.5\mu_B$ for Mn^{3+} and Mn^{4+} ions, respectively. The total magnetic moment for the monomer is $9\mu_B$, in good agreement with experiment. The highest occupied molecular orbital–lowest unoccupied molecular orbital (HOMO-LUMO) gap for majority (minority) spin is 1.02 eV (2.42 eV). The energy difference between the minority (majority) LUMO and the majority (minority) HOMO is 1.17 eV (2.28 eV), which ensures that the system is stable with respect to the total magnetic moment. As clearly seen in Fig. 2, right below the Fermi level for majority spins the projected $Mn^{3+}(3d)$ DOS is dominant over the projected $Mn^{4+}(3d)$ density of states (DOS), while for minority spins the opposite trend is observed. This confirms the experimental picture of three Mn^{3+} spins antiferromagnetically coupled to a Mn^{4+} spin.

We calculate the binding energy by subtracting the dimer energy from twice the monomer energy. We find that the dimer is stable for both the CDC and EDC. For the CDC (EDC), the binding energy is about 0.16 eV (0.78 eV). The magnitude of the binding energy suggests attractive electrostatic interactions between different monomers. The discrepancy between the binding energy for the CDC and that for the EDC may be attributed to our substitution of an ethyl group for hydrogen in the CDC and/or the fact that the plane where a pyridine ring sits is different for both geometries. To check the former possibility, we calculate the binding energy of the EDC terminated by hydrogen, and obtain 0.45 eV. We have also verified that the conformation of a pyridine ring for the EDC is slightly different from that for the CDC. Thus, the discrepancy arises from both reasons.

We have calculated the monomeric MAE in zero mag-

TABLE I. Binding energy, monomeric magnetic anisotropy barrier (MAE), and antiferromagnetic exchange constant J for the CDC with the distance between the two central Cl's held as the experimental value, $d = 3.86$ Å [DFT(1)], the EDC with $d = 3.86$ Å [DFT(2)], and the same as DFT(2) except that ethyl is replaced by hydrogen [DFT(3)]. DFT(4), DFT(5), and DFT(6) denote the same as DFT(2) except that $d = 3.86$ Å $+ 1$ bohr, $d = 3.86$ Å $- 0.5$ bohr, and $d = 3.86$ Å $- 1$ bohr, respectively. The experimental values are from Ref. 6. The numerical uncertainty in the estimated values of J is ~ 0.04 K.

	Binding energy (eV)	MAE/monomer (K)	Exchange J (K)
DFT(1)	0.16	11.3	0.24
DFT(2)	0.78	11.6	0.27
DFT(3)	0.45	10.9	
DFT(4)		11.7	0.10
DFT(5)		11.6	0.47
DFT(6)		11.7	0.81
Expt. (Ref. 6)		14.4	0.1

FIG. 3. (Color online) Logarithm of exchange constant J as a function of the monomer-monomer distance relative to the experimental value. The numerical uncertainty in J is ~ 0.04 K. The slope of the curve is about -2.

netic field for both the CDC and EDC with the assumption that spin-orbit coupling is a major contribution to the MAE. For this calculation, we follow the procedure developed in Ref. 12. Our calculations show that the Mn_4 monomer has uniaxial anisotropy along the threefold axis (the bond between Mn^{4+} and Cl in the cubane), in agreement with experiment.[5,6] For uniaxial systems, the energy shift Δ due to the spin-orbit interaction can be simplified to $-\gamma_{zz}\langle S_z \rangle^2$ up to constant terms independent of $\langle S_z \rangle$ if the z axis is assigned as the easy axis.[12] Then the classical barrier (MAE) to be overcome to monomer magnetization reversal $M_z = +9/2$ to $M_z = -9/2$ is $\gamma_{zz}[(9/2)^2 - (1/2)^2]$. For the CDC (EDC) monomer, the MAE is 11.3 K (11.6 K), which is close to that for the hydrogenated EDC monomer. As shown in Table I, all these numbers are close to the experimental value of 14.4 K. The difference between our estimated MAE and the experimental value might be ascribed to other effects on the barrier such as spin-vibron coupling.[13]

To calculate the exchange-coupling constant J between monomers, we assume that a monomer is an ideal $S = 9/2$ object and that its effective spin is aligned along the easy axis and of Ising type (either $M_z = +9/2$ or $-9/2$). Then we calculate self-consistently energies of ferromagnetic (parallel monomeric spins) and antiferromagnetic configuration (antiparallel monomeric spins) of the dimer, and take a difference δ between the two energies. We find that the antiferromagnetic configuration is favored. The antiferromagnetic exchange constant J is determined from $\delta = 2J(9/2)^2$. For the CDC, the energy difference is 31 microHartree, so that $J = 0.24$ K, while for the EDC, $J = 0.27$ K. These can be compared to the experimentally measured value of $J = 0.1$ K.[6] The numerical uncertainty in the total-energy difference for our DFT calculations is at most 5 microHartree, which can be translated to the uncertainty in the exchange J as 0.04 K. We achieve high accuracy in the total-energy difference, because we use exactly the same optimized dimer geometry with the same parameter values for a self-consistent approximation except for the effective spin configurations of mono-
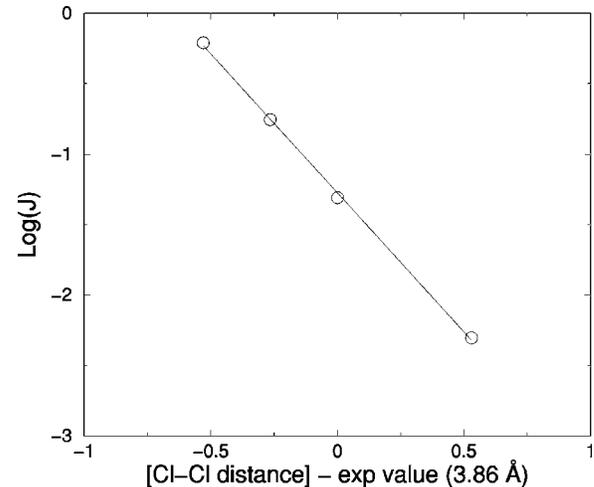
mers. Although our DFT estimated value of J is somewhat higher than the experimental value, this may be acceptable considering the assumptions we made, and the fact that DFT calculations often overestimate exchange interactions. In some cases, the PBE generalized-gradient approximation may not fully cancel the self-interaction in the Coulomb potential. Therefore, the electrons in our calculations are slightly more diffuse, which should lead to overestimated exchange interaction. This may be improved by including the electron correlations in Mn atoms using the dynamical mean-field theory[14] or the LDA+U method.[15] The LDA+U calculations on the SMM Mn_{12} showed that the intramolecular exchange interactions decrease on increasing the value of U.[16]

It is interesting to examine whether the exchange interaction varies significantly with the monomer-monomer separation. We consider the case that each monomer is displaced toward or away from the center of mass of the dimer along the easy axis. Then we calculate the exchange constant J for the EDC dimer with three different monomer-monomer distances from the experimentally measured value. The monomer-monomer distance is varied by changing the central Cl-Cl distance with a monomer geometry fixed. If the central Cl-Cl bond length increases by 1 bohr, then J decreases down to 0.10 K. If the bond length decreases by 0.5 bohr (1 bohr), J increases to 0.47 K (0.81 K). Table I summarizes the separation dependence of J and of the monomeric MAE. As shown in Table I, the monomeric MAE does not depend on the exchange interaction between monomers, because the monomer geometry has not changed during this process. Figure 3 shows that J increases exponentially with decreasing separation distance. This tells us how quickly the overlaps of neighboring wave functions decrease with increasing distance. We have decomposed the J values into kinetic, Coulombic, and exchange-correlation contributions. The kinetic contribution is an order of magnitude larger than the total value of J, and it is significantly canceled by the exchange-correlation contributions to the J value.

Since we estimated the anisotropy barrier and exchange

constant, we can construct a model Hamiltonian for the dimer according to

$$\mathcal{H} = -\gamma_{zz}(S_{1z}^2 + S_{2z}^2) + J\vec{S}_1 \cdot \vec{S}_2, \qquad (1)$$

where the uniaxial anisotropy parameter $\gamma_{zz} = 0.58$ K and $J = 0.27$ K. To determine whether our values of γ_{zz} and J can reproduce the experimental values of the resonant tunneling fields (Fig. 4 in Ref. 6), we calculate these fields using exact diagonalization of Hamiltonian (1). Although it is crucial to include some small transverse terms in the Hamiltonian (such as transverse anisotropy and transverse fields) for calculations of tunnel splittings, the transverse terms do not affect the resonant fields much. Table II summarizes the resonant fields for some low-energy states for three different values of γ_{zz} and J: (1) the experimental values $\gamma_{zz} = 0.72$ K, $J = 0.1$ K; (2) $\gamma_{zz} = 0.58$ K, $J = 0.27$ K; and (3) slightly modified version of our DFT results $\gamma_{zz} = 0.58$ K, $J = 0.1$ K. Let us focus on two tunnelings which were prominent in the experimental measurements: $|M_1 = 9/2, M_2 = 9/2\rangle \rightarrow |M_1 = 9/2, M_2 = -9/2\rangle$ and $|9/2, -9/2\rangle \rightarrow |-9/2, -9/2\rangle$, where M_1 and M_2 are the eigenvalues of the spin operator projected along the easy axis for each monomer. For these two tunnelings, the resonant fields are solely determined by J and are independent of γ_{zz}: $B_{res} \approx \mp 9J/(2g\mu_B)$. Therefore, the model Hamiltonian (1) with our estimated values will not quantitatively reproduce the experimental resonant fields. However, in this case (when γ_{zz} becomes comparable to J), we notice that the hysteresis loop exhibits richer features, such as more magnetization steps, before magnetic field reversal. Since DFT often overestimates exchange interactions, we also calculate the resonant fields with J decreased to 0.1 K and γ_{zz} fixed to examine if agreement with experiment improves. We find that some resonances agree with experiment and some do not agree.

In summary, we have calculated optimized geometries for a monomer and dimer of the SMM Mn$_4$ using DFT. For both

TABLE II. Initial $|M_1, M_2\rangle$ and final states $|M_1', M_2'\rangle$ participating in quantum tunneling at resonant fields B_{res}. This was calculated by exact diagonalization of Hamiltonian (1). M_1 and M_2 are the projected magnetic moments along the easy axis for each monomer. For clarity, degeneracy in initial/final states is not listed. Only for the case with $\gamma_{zz} \gg J$, the initial/final states are eigenstates of Hamiltonian (1). The third and fourth resonances are from one degenerate state to another degenerate state, and they are split due to transverse terms in the exchange interaction. The same logic is applied to the last two resonances. B_{res}^{Exp} is the resonant field for $\gamma_{zz} = 0.72$ K and $J = 0.1$ K. B_{res}^{DFT} is for $\gamma_{zz} = 0.58$ K and $J = 0.27$ K. B_{res}^{Mod} is for $\gamma_{zz} = 0.58$ K and $J = 0.1$ K.

Initial	Final	B_{res}^{Exp}(T)	B_{res}^{DFT}	B_{res}^{Mod}
$\left|\frac{9}{2}, \frac{9}{2}\right\rangle$	$\left|\frac{9}{2}, -\frac{9}{2}\right\rangle$	−0.335	−0.915	−0.335
$\left|\frac{9}{2}, \frac{9}{2}\right\rangle$	$\left|\frac{9}{2}, -\frac{7}{2}\right\rangle$	0.20	−0.495	0.095
$\left|\frac{9}{2}, -\frac{7}{2}\right\rangle$	$\left|-\frac{9}{2}, -\frac{7}{2}\right\rangle$	0.23	0.625	0.23
$\left|\frac{9}{2}, -\frac{7}{2}\right\rangle$	$\left|-\frac{9}{2}, -\frac{7}{2}\right\rangle$	0.305	0.83	0.305
$\left|\frac{9}{2}, -\frac{9}{2}\right\rangle$	$\left|-\frac{9}{2}, -\frac{9}{2}\right\rangle$	0.34	0.92	0.34
$\left|\frac{9}{2}, \frac{9}{2}\right\rangle$	$\left|\frac{9}{2}, -\frac{5}{2}\right\rangle$	0.735	−0.08	0.525
$\left|\frac{9}{2}, -\frac{9}{2}\right\rangle$	$\left|-\frac{9}{2}, -\frac{7}{2}\right\rangle$	0.835	1.24	0.73
$\left|\frac{9}{2}, -\frac{9}{2}\right\rangle$	$\left|-\frac{9}{2}, -\frac{7}{2}\right\rangle$	0.915	1.465	0.815

the CDC and EDC, we calculated binding energy, monomeric MAE, and the exchange interaction between monomers. The binding interaction between monomers is electrostatic. Our calculated anisotropy barrier is close to the experimental value. The exchange interaction between monomers is twice or three times larger than the experimental value. Overall, our DFT calculations are in qualitative accord with experiment.

*Electronic address: park@dave.nrl.navy.mil

[1] T. Lis, Acta Crystallogr., Sect. B: Struct. Crystallogr. Cryst. Chem. **B36**, 2042 (1980).

[2] K. Wieghart, K. Pohl, I. Jibril, and G. Huttner, Angew. Chem., Int. Ed. Engl. **23**, 77 (1984).

[3] J. Villain, F. Hartman-Boutron, R. Sessoli, and A. Rettori, Europhys. Lett. **27**, 159 (1994); E. M. Chudnovsky and J. Tejada, *Macroscopic Quantum Tunneling of the Magnetic Moment*, Cambridge Studies in Magnetism Vol. 4 (Cambridge University Press, Cambridge, 1998), and references therein.

[4] R. Sessoli, D. Gatteschi, A. Caneschi, and M.A. Novak, Nature (London) **365**, 141 (1993); J.R. Friedman, M.P. Sarachik, J. Tejada, and R. Ziolo, Phys. Rev. Lett. **76**, 3830 (1996); W. Wernsdorfer and R. Sessoli, Science **284**, 133 (1999).

[5] D.N. Hendrickson, G. Christou, E.A. Schmitt, E. Libby, J.S. Bashkin, S. Wang, H.-L. Tsai, J.B. Vincent, P.D.W. Boyd, J.C. Huffman, K. Folting, Q. Li, and W.E. Streib, J. Am. Chem. Soc. **114**, 2455 (1992); R. S. Edwards, S. Hill, S. Bhaduri, N. Aliaga-Alcalde, E. Bolin, S. Maccagnano, G. Christou, and D. N. Hendrickson, Polyhedron (to be published).

[6] W. Wernsdorfer, N. Aliaga-Alcade, D.N. Hendrickson, and G. Christou, Nature (London) **416**, 406 (2002).

[7] W. Kohn and L.J. Sham, Phys. Rev. **140**, A1133 (1965).

[8] M.R. Pederson and K.A. Jackson, Phys. Rev. B **41**, 7453 (1990); K.A. Jackson and M.R. Pederson, *ibid.* **42**, 3276 (1990); D. V. Porezag, Ph.D. thesis, Chemnitz Technical Institute, 1997.

[9] J.P. Perdew, K. Burke, and M. Ernzerhof, Phys. Rev. Lett. **77**, 3865 (1996).

[10] K. Park, M.R. Pederson, and N. Bernstein, cond-mat/0307145 (unpublished).

[11] D. Porezag and M.R. Pederson, Phys. Rev. A **60**, 2840 (1999).

[12] M.R. Pederson and S.N. Khanna, Phys. Rev. B **60**, 9566 (1999).

[13] M.R. Pederson, N. Bernstein, and J. Kortus, Phys. Rev. Lett. **89**, 097202 (2002).

[14] A. Georges, G. Kotliar, W. Krauth, and M.J. Rozenberg, Rev. Mod. Phys. **68**, 13 (1996).

[15] V.I. Anisimov, F. Aryasetiawan, and A.I. Lichtenstein, J. Phys.: Condens. Matter **9**, 767 (1997).

[16] D.W. Boukhvalov, A.I. Lichtenstein, V.V. Dobrovitski, M.I. Katsnelson, B.N. Harmon, V.V. Mazurenko, and V.I. Anisimov, Phys. Rev. B **65**, 184435 (2002).